Asian Journal of Chemistry; Vol. 33, No. 3 (2021), 570-576

ASIAN JOURNAL OF CHEMISTRY

https://doi.org/10.14233/ajchem.2021.23041

Chemical and Plant Mediated Synthesis of La_2O_3 Nanoparticles and Comparison of their Structural, Antibacterial, Photocatalytic and Optical Properties

A. SWETHARANYAM and R. KUNJITHAM*

P.G. & Research Department of Chemistry, Poompuhar (Autonomous) College (Affiliated to Bharathidasan University, Tiruchirappalli), Melaiyur-609107, India

*Corresponding author: E-mail: kunjithamr@gmail.com

Received: 26 October 2020; *Accepted*: 5 January 2021; *Published online*: 16 February 2021; AJC-20251

The La_2O_3 nanoparticles have been synthesized successfully with a chemical and biosynthesized method. The optical bandgap energy and of chemically synthesized or biosynthesized (*M. oppositifolia* and *T. portlacaustrum* leaf extract) La_2O_3 nanoparticles was calculated from UV-visible absorption between 5.10, 4.26 and 4.46 eV. The good polycrystalline cubic nature of synthesized La_2O_3 nanoparticles was evident from the bright circular SAED pattern, consistent with the XRD outcome. It is clear that the non-polar extracts could function as stabilizers for La_2O_3 nanoparticles through attachment to the counterions. The La_2O_3 nanoparticles have been used as efficient photocatalyst to degrade acid black 1 dye under sunlight irradiation. Besides, this biocatalyst showed excellent ability to degrade biosynthesized La_2O_3 nanoparticles (*T. portlacaustrum*) under visible light irradiation 87%. Synthesis of La_2O_3 nanoparticles by green chemistry process presented good antibacterial activity against Gram-negative and Gram-positive bacteria.

Keywords: La_2O_3 nanoparticles, *M. oppositifolia*, *T. portlacaustrum*, Photocatalytic degradation, Antibacterial activity.

INTRODUCTION

Today's industrial revolution is heavily detrimental to the entire world. Greater and greater variety of contaminants continue being generated by fashion, textile and dyeing industries. These substances are highly carcinogenic and genotoxic [1,2] and causing nitrogen runoff, eutrophication and high demand for oxygen in water (BOD). Besides that, these compounds have strong photosynthetic ability which harms the whole ecosystem [3,4]. There are many environmental risks because of organic dyes [5]. To resolve this problem, researchers are employing photocatalytic processes for the degradation of organic pollutants in industrial waste water before discharging them. Although various chemical and physical treatments processes are available for the treatment of textile effluents but these technologies only produce non-biodegradable contaminants and require costly treatment procedures [6,7]. In addition, these conventional techniques such as coagulation, flocculation, membrane separation and absorption methods are also ineffective for the removal of complex organic compounds [8,9]. However, advanced oxidation processes (AOPs) are highly efficient novel methods and the least expensive alternative method for the wastewater treatment process. Faster degradation of dye is affected by the high oxidative powers of OH radicals and it can be further enhanced by UV-visible radiation that generates OH radicals. A major advantage of the photocatalytic process is that there is no secondary waste treatment and does not need expensive oxidizing chemicals [10,11].

Various photocatalysts have been used in the photocatalytic degradation process. As a result of the unique configuration of 4*f*-electrons, lanthanides are an attractive element with unique optical, catalytic and magnetic properties [12,13]. Lanthanum oxide (La_2O_3) has undergone considerable research among the various lanthanum based materials, with its applications as a door-insulator and superconductor, hydrogen storage, an electrode and as a serpentine material [14]. La_2O_3 also received considerable attention because of its extensive usage in piezoelectricity, galvanothermic and thermoelectricity, and light emitting phosphors, catalysts and automotive gas convector components [15].

The electronic structure of semiconductor is significant for photocatalysis. There are electrons and holes in the valence

band without excitation and energy is less than 3.5V. When semiconductor surface is exposed to light, then electrons are transferred from the valence band to the conduction band, and leave behind holes (electron-hole pairs) on the valence band. The electrons and holes migrates to the surface of the semiconductor and causes the reactants to be partially oxidized on the surface of the semiconductor [16,17]. Compared to hydrogen and ozone, the reduction and oxidation potential of these free radicals generated by sunlight is much higher. These electron-hole pairs are acting as a strong redox system. Light produced UV photodissociation of OH^- and H_2O molecules on the photo-produced La_2O_3 surfaces [18]. The electrons in the conduction band can facilitate reduction of O_2 molecules, which exist in the air is on the TiO_2 surface and form peroxyl radicals. These nitric oxide radicals in turn oxidize and degrade organic/inorganic materials. The two basic photocatalytic mechanisms are the reduction and oxidation reactions.

La_2O_3 nanoparticles can be produced by different techniques like physical and chemical methods. Unfortunately these methods are either very expensive or may involve toxic chemicals for synthesis. Therefore, there is also a need to develop eco-friendly methods/techniques without using hazardous chemicals [19]. Green synthesis of La_2O_3 nanoparticles is a fast increasing and economical research in nanoparticle synthesis. Many plant extracts can be used as a capping as well as reducing agents for the synthesis of nanoparticles, excluding the use of hazardous chemical agents and other purification techniques [20]. Herein, we used *M. oppositifolia* and *T. portlacastrum* leaf extract for the preparation of La_2O_3 nanoparticles. The synthesized nanoparticles were characterized with XRD, FT-IR, HR-TEM, UV-DRS and PL measurements. In addition, both synthesized nanoparticles were also evaluated for photocatalytic, antibacterial and antioxidant activities.

EXPERIMENTAL

Lanthanum nitrate, sodium hydroxide, organic dyes and different reagents were purchased from Sigma-Aldrich Ltd., India. Distilled water was used throughout the experiment. At room temperature, Shimadzu 6000 X-ray diffraction (λ = 1.5406 Å) was studied with the X-ray crystallography analysis of nanoparticles. The optically detected signals were recorded using a Jasco V-670 spectrophotometer. The photoluminescence (PL) studies were performed at room temperature with an excitation wavelength of 325 nm by Chlorolog 3-Horiba Jobin Yuen. Particle shapes were stabilized by SEM and HR-TEM (Hitachi S-4500 SEM engine). FTIR analysis was performed using a KBr pallet on FT-IR (2000) by Perkin-Elmer at room temperature in the 4000-400 cm^{-1} range in order to identify the groups present on the synthesized nanoparticles.

Preparation of leaf extract: Fresh leaves of *M. oppositifolia* and *T. portlacastrum* were collected and washed three to five times with faucet water and then flushed three times with 10 g of the potting mixture. Distilled water (100 mL) was added to the cup with the basil leaves cut into pieces. The sugar solution was heated at 80 ºC for 25 min and then the precipitate was removed with filter paper.

Synthesis La_2O_3 NPs by chemical method: Lanthanum nitrate (0.1 M) was dissolved in distilled water with constant stirring for 30 min at room temperature. Toa a above solution, 0.2 M of aqueous NaOH solution was added by dropwise at room temperature with a constant stirrer continuous at 90 ºC. When it was cooled down to room temperature, a white gel was formed. The gel was warmed at 80 ºC in the dry oven for 12h, a dry gel was obtained and then milled in mortar. The dry gel powder was heated at 450 ºC in air so as to remove the organic substance and decompose lanthanum nitrate. Finally, it was calcined at 750 ºC and the La_2O_3 NPs were obtained.

Biosynthesis of La_2O_3 NPs: Lanthanum nitrate solution (0.1 M) was added dropwise to 10 mL of leaf extract separately and then stirred at 85 ºC for 2 h. The mixture was extracted and evaporated in an ultrasonic bath. Then the powder of calcined gel was dried and calcined for 2 h at 750 ºC until La_2O_3 NPs was formed.

Photocatalytic activity: The photocatalytic properties of synthesized nanoparticles were achieved by illumination under sunlight by Acid black 1 dye. The dye solution was prepared by dissolving 10 mL of dye in 500 mL of water. The suspension of synthesized nanoparticles (0.06 g samples of 100 mL of dye solution) in the dye solution was stirred for 60 min in the dark before illumination to balance the solution. As the solution was made more balanced, the coloured flame was lit inside the furnace. UV-VIS spectrophotometer concentration of acid black 1 in water samples was measured. The percent absorption of acid black 1 dye at the catalyst surface was then calculated.

Antibacterial activity: Kirby Bauer's diffusion method [21] was applied to determine the antibacterial properties of biosynthesized and chemically synthesized La_2O_3 nanoparticles.The liquid supplement was suspended in a sterile microbe rich broth. A sterile steel surgical cotton drill was used to dispense the microbes into the agar. The aseptic state in the source had been added 50 and 100 µL samples and 25 µg of ciprofloxacin were used as control. At 35 ºC for 24 h, the test plates were grown and the square width was then measured.

RESULTS AND DISCUSSION

XRD analysis: X-ray diffraction analysis was employed to study the average crystallite size and structural properties of prepared La_2O_3 nanoparticles. The diffraction peaks and their relative intensities of all samples were in good agreement with the standard JCPDS card no.05.0602. Hence, the observed patterns can be clearly endorsed to the presence of hexagonal structure. Biosynthesized (*M. oppositifolia* and *T. portlacastrum* leaf extracts) La_2O_3 nanoparticles, the XRD peaks for (100), (002) and (101) planes indicates the formation lanthanum oxide of phase pure hexagonal structure and some peaks intensity are high as compared to chemically synthesized La_2O_3 nanoparticles. The high intensity of peaks suggests that the growth of nanoparticles has taken place along this direction of crystallization of La_2O_3 nanoparticles. No additional peaks were observed, which indicates all the samples very high purity (Fig. 1).

The average crystalline size of both biosynthesized and chemically nanoparticles was determined from the full-width at half maximum by applying to Scherrer's formula [22]:

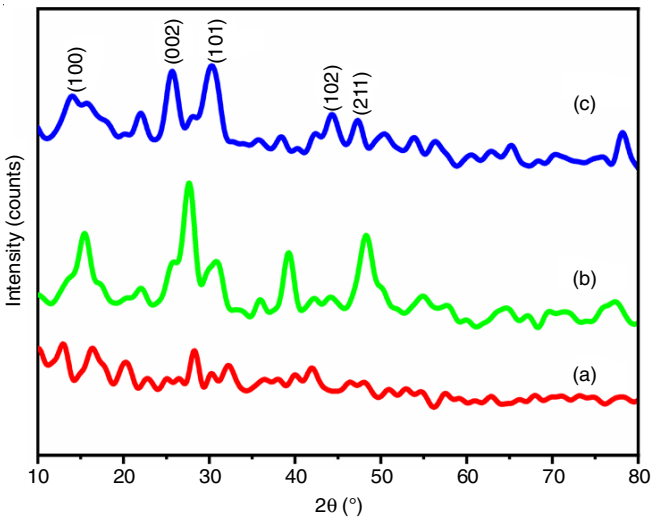

Fig. 1. X-ray diffraction patterns of (a) chemical synthesized La_2O_3 NPs, (b) *T. portlacastrum* and (c) *M. oppositifolia* mediated biosynthesized La_2O_3 NPs

$$D = \frac{0.9\lambda}{\beta\cos\theta}$$

The lattice constant (a), dislocation density (δ) and micro-strain (ε) were calculated using the following equations [22]:

$$\frac{1}{d^2} = \frac{4}{3}\left(h^2 + hk + \frac{k^2}{a^2}\right) + \frac{l^2}{c^2}$$

$$\varepsilon = \frac{\beta\cos\theta}{4}$$

$$\delta = \frac{1}{D^2}\ \text{lin/m}^2$$

where D is the crystallite size, λ is the wavelength of X-ray source, β is the full width at half maximum and θ is the Braggs diffracting angle.

The bandgap energy of SPR was calculated using eqn 4:

$$E = \frac{hc}{\lambda}$$

where λ is the wavelength, h is the Planks constant and C is the velocity of light. The bandgap values of chemically and biosynthesized (*M. oppositifolia* and *T. portlacastrum* leaf extract) La_2O_3 NPs are shown in Table-1, along with the other physical parameters. It can be observed that the crystalline size of biosynthesized (*T. portlacastrum*) La_2O_3 NPs is small as compared to chemically prepared La_2O_3 NPs and *M. oppositifolia* leaf extract mediated nanoparticles. However, the dislocation density was found to be maximum in biosynthesized (*T. portlacastrum* leaf extract) La_2O_3 NPs. As crystalline size decreases, the dislocations density found to be increased, thus by increasing the yield strength of the material requires the higher shear stress for the movement of dislocation [23].

Morphological (HR-TEM) analysis: The HR-TEM images of chemically synthesized La_2O_3-NPs and biosynthesized (*M. oppositifolia* and *T. portlacastrum* leaf extract) La_2O_3 NPs is shown in Figs. 2-4. The synthesized nanoparticles were found to be large and uniform in shape. Particles which are almost similar and uniform in size 37, 30 and 27 nm for chemically synthesized La_2O_3 NPs and biosynthesized (*M. oppositifolia* and *T. portlacastrum* leaf extract) La_2O_3 NPs, respectively. It is also clear from the HR-TEM results that biosynthesized La_2O_3 NPs have reduced particle size. The interfering distance of chemically synthesized La_2O_3 NPs and biosynthesized La_2O_3 NPs was measured to be 0.32, 0.27 and 0.27 nm, which corresponds to be (002) planes samples.

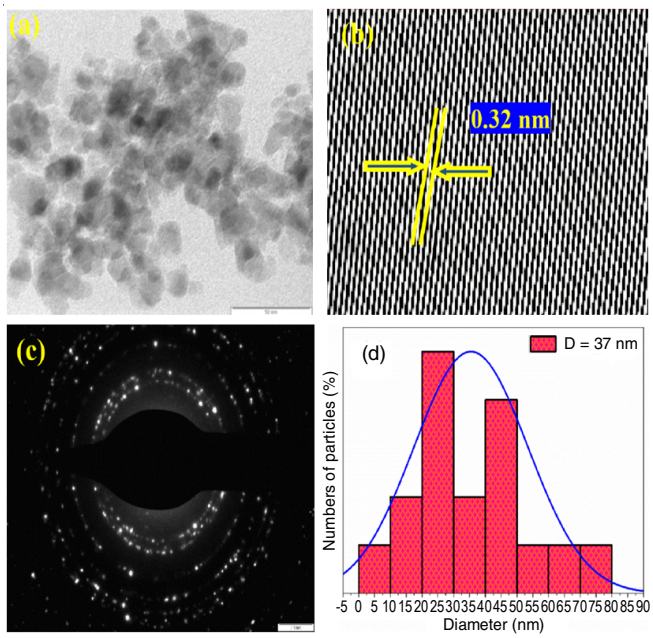

Fig. 2. (a) HR-TEM image (b) lattice fringes (c) SAED pattern (d) particle size of chemically synthesized La_2O_3 NPs

TABLE-1
DIFFERENT STRUCTURE PARAMETERS OF CHEMICALLY SYNTHESIZED AND BIO SYNTHESIZED (*M. oppositifolia* AND *T. portlacastrum* LEAF EXTRACT) La_2O_3 NPs

Samples	2θ	FWHM	Miler indices (hkl)	Average micro strain (ε)	Average dislocation density (δ)	Average crystalline size (D)
Chemically synthesized	37.140	0.2478	(102)	9.06	18.96	40
	22.067	0.2108	(002)			
	29.784	0.2048	(101)			
M. oppositifolia	37.294	0.2106	(102)	15.06	32.27	29
	22.964	0.1998	(002)			
	29.348	0.1968	(101)			
T. portlacastrum	38.014	0.2371	(102)	11.91	26.92	32
	22.491	0.1970	(002)			
	29.943	0.1997	(101)			

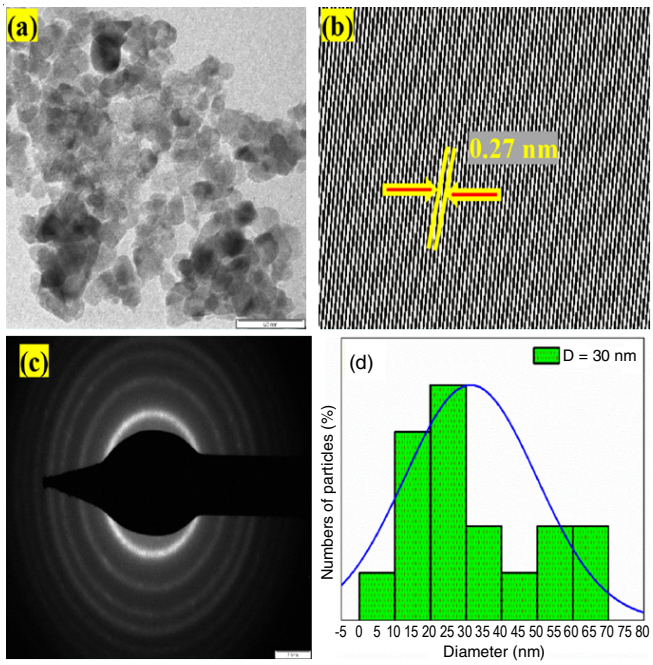

Fig. 3. (a) HR-TEM image (b) lattice fringes (c) SAED pattern (d) particle size of biosynthesized (*M. oppositifolia*) LaO_2 NPs

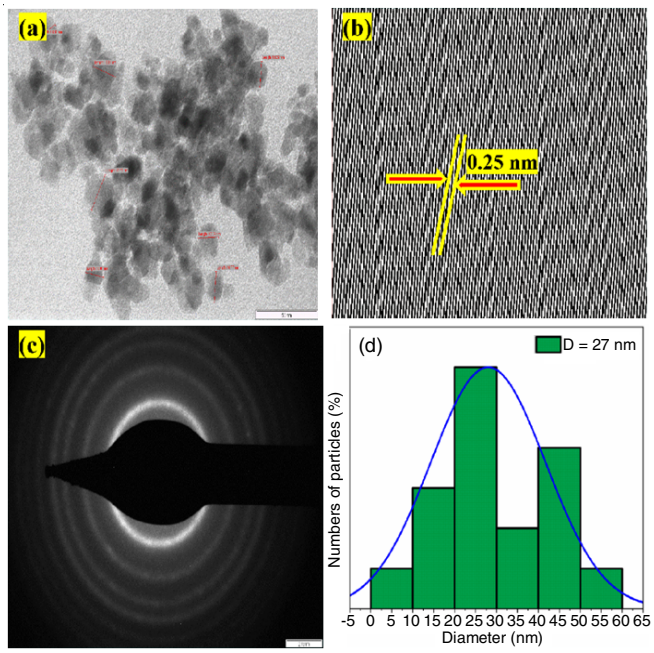

Fig. 4. (a) HR-TEM image (b) lattice fringes (c) SAED pattern (d) particle size of biosynthesized (*T. portlacastrum*) LaO_2 NPs

FT-IR analysis: The FT-IR spectra of *M. oppositifolia* and *T. portlacastrum* leaf extracts are shown in Fig. 5. The absorption peaks at 3493.12, 2966, 2415.48, 1486.12, 1202.74 and 650.24 cm^{-1} are the characteristic –OH stretching vibration and –CH stretching vibrations [24-27]. A band around 1486.12 cm^{-1} can be assigned to the amide I and II N-H curves resulting from carbonyl stretching and peptide protein coupling. The presence of amides and carboxyl groups in both plants leaf extracts has been confirmed from the FT-IR analysis. This group is responsible for the bioreduction of lanthanum nitrate to nanoparticles of lanthanum oxide.

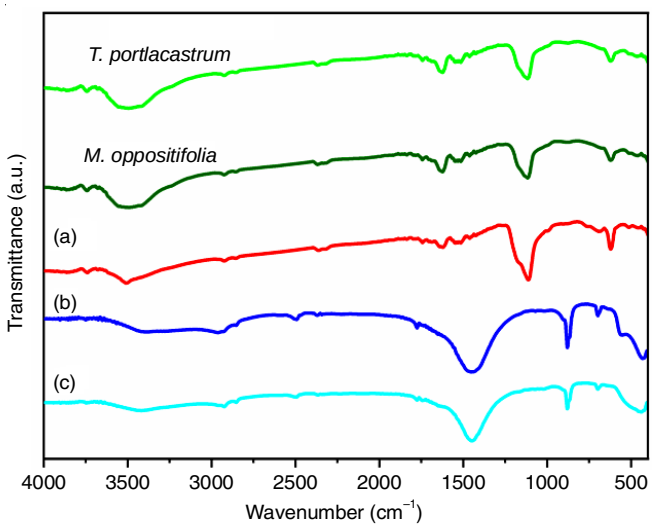

Fig. 5. FT-IR spectra of (a) chemically synthesized La_2O_3 NPs; (b-c) biosynthesized (*M. oppositifolia* and *T. portlacastrum* leaf extract) La_2O_3 NPs

The chemically synthesized La_2O_3 NPs exhibited the absorption peaks 3396.28, 1469.27, 1175.15 and 842.87 cm^{-1}. The band around 1469.27 cm^{-1} confirmed the C-H deformation vibration of the alkane group. The bands around 1175.15 cm^{-1} are attributed to the –OH bending vibration and C-H stretching which clearly indicated the existence of a large number of hydroxyl groups [28,29]. The bands at 850-800 and 450-400 cm^{-1} is attributed to the M–O band [30]. However, an important enlargement of the spectral area was observed in case of the biosynthesized La_2O_3 nanoparticles (Table-2). Flavonoids are really helpful in reducing lanthanum nitrate. The La_2O_3 NPs molecules have peaks in the biosynthesized particles which are slightly modified.

TABLE-2
KEY IR BANDS (cm^{-1}) OF CHEMICALLY AND BIOSYNTHESIZED (*M. oppositifolia* AND *T. portlacastrum* LEAF EXTRACT) La_2O_3 NPs

Wavenumber (cm^{-1})			Functional group
La_2O_3 NPs			
Chemically	*M. oppositifolia*	*T. portlacastrum*	
3496	3488	3466	O-H
2946	2958	2955	C-H stretching
2741	2757	2739	Aromatic bands
2499	2485	2488	C–H stretching
1402	1457	1424	C-C vibrations
–	757	764	C-H stretching
–	597	592	C=O vibrations

Optical analysis: In the optical absorbance spectrum of La_2O_3 NPs at 200-800 nm range was recorded using a UV-visible spectrophotometer. Fig. 6 shows the absorption peaks of chemically and biosynthesized La_2O_3 NPs at about 247, 278 and 282 nm, respectively. In biosynthesized samples, the absorption peak at 278 and 282 nm shifted towards the higher wavelength side (red shift) and also the intensity was increased when compared to the chemically synthesized La_2O_3 NPs (247 nm). The changes in the absorption peaks, due to aggregation

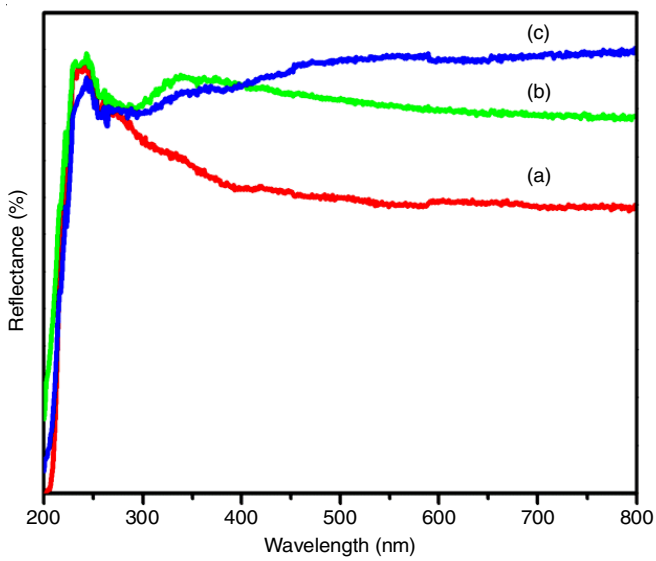

Fig. 6. UV-Vis DRS spectra of (a) chemically synthesized La_2O_3 NPs and (b-c) biosynthesized (*M. oppositifolia* and *T. portlacastrum* leaf extract) La_2O_3 NPs

are observable as an intensity increase in the red/infrared region of the spectrum [23]. Reduction of La_2O_3 NPs during exposure to the plant leaf extracts was followed by colour change and thus UV-Vis spectrum [31].

The bandgap of chemically and biosynthesized La_2O_3-NPs and biosynthesized (*M. oppositifolia* and *T. portlacastrum* leaf extract) La_2O_3 NPs values were found to be 5.10, 4.26 and 4.46 eV, respectively (Fig. 7). From the plot, the bandgap of chemically synthesized of La_2O_3 NPs was found to be around 5.10 eV, which is blue-shifted evidently compared with that of the biosynthesized La_2O_3 nanoparticles. This means blue shift in the absorption is due to the quantum confinement effect [32].

Photoluminescence studies: The photoluminescence (PL) spectrum of chemically and biosynthesized (*M. oppositifolia*

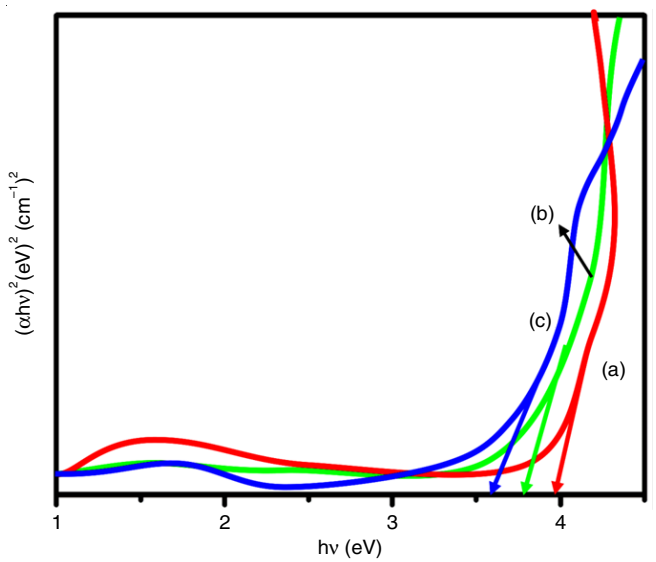

Fig. 7. Bandgap energy of chemically synthesized La_2O_3 NPs and biosynthesized (*M. oppositifolia* and *T. portlacastrum* leaf extract) La_2O_3 NPs

and *T. portlacastrum* 2 leaf extract) La_2O_3 NPs with 360 nm as excitation wavelength is shown in Fig. 8. All the spectra exhibit an excitonic peak in ultraviolet region and defect related peak in the visible region, which is essentially related to the lanthanum oxide defects. Chemically synthesized La_2O_3 NPs exhibit a peak around 357 nm associated with near band ultra violet emission. This ultraviolet band corresponds to the near band-edge (NBE) emission, which is related essentially to the recombination of free excitations [33]. A low PL intensity of the biosynthesized La_2O_3 NPs observed as compared to the chemically synthesized La_2O_3 NPs is due to the oxygen defects [34]. Biosynthesized La_2O_3 NPs spectrum exhibits two emission peaks, one located at around 342 nm corresponding to the near bandgap excitoinc emission and the other is located at around 372 nm attributed to the presence of singly ionized oxygen vacancies [35]. Emissions are caused by radioactive recombination of a photosensitive hole with an electron occupying the oxygen vacuum.

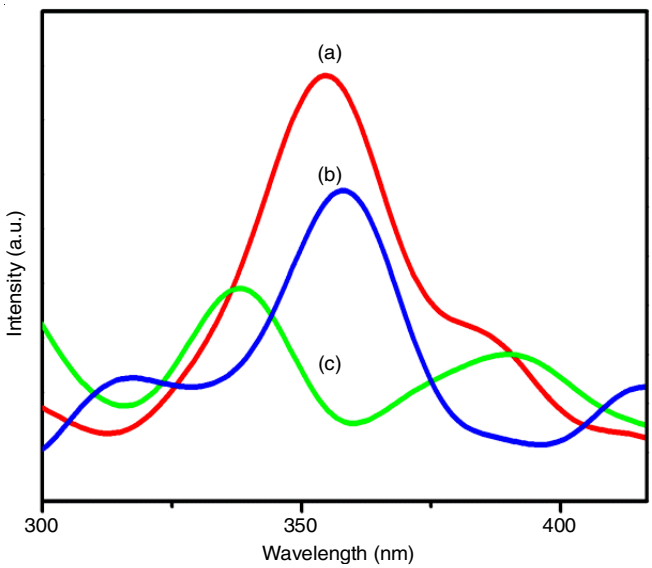

Fig. 8. Photoluminescence spectra of chemically synthesized La_2O_3 NPs and biosynthesized (*M. oppositifolia* and *T. portlacastrum* leaf extract) La_2O_3 NPs

Photocatalytic activity: The photocatalytic activity is assessed by means of a chemically and biosynthesized La_2O_3 nanoparticles towards the acid black 1 dye solution. The UV-Vis spectra were recorded at various intervals of 0, 15, 30, 45, 60, 75 min. The peak of absorption of UV-Vis at 632 nm refers to the acid black 1 dye colour, which is reduced to dark blue by electron transfer. That is why, it was observed that the peak was reducing from the maximum (Fig. 9), indicated that less degradation of acid dyes was taking place. Utilizing chemical synthesis towards La_2O_3 NPs requires multiple processes. This will happen because of defects in the crystalline structure of La_2O_3 NPs. It can be seen that *M. oppositifolia* leaf extract induced La_2O_3 NPs with an 85% degradation had the highest stability as compared to *T. portlacastrum* leaf extract induced La_2O_3 NPs (Table-3).

Mechanism: Enhanced photocatalytic activity for the biosynthesized La_2O_3 NPs are due to the extended surface area

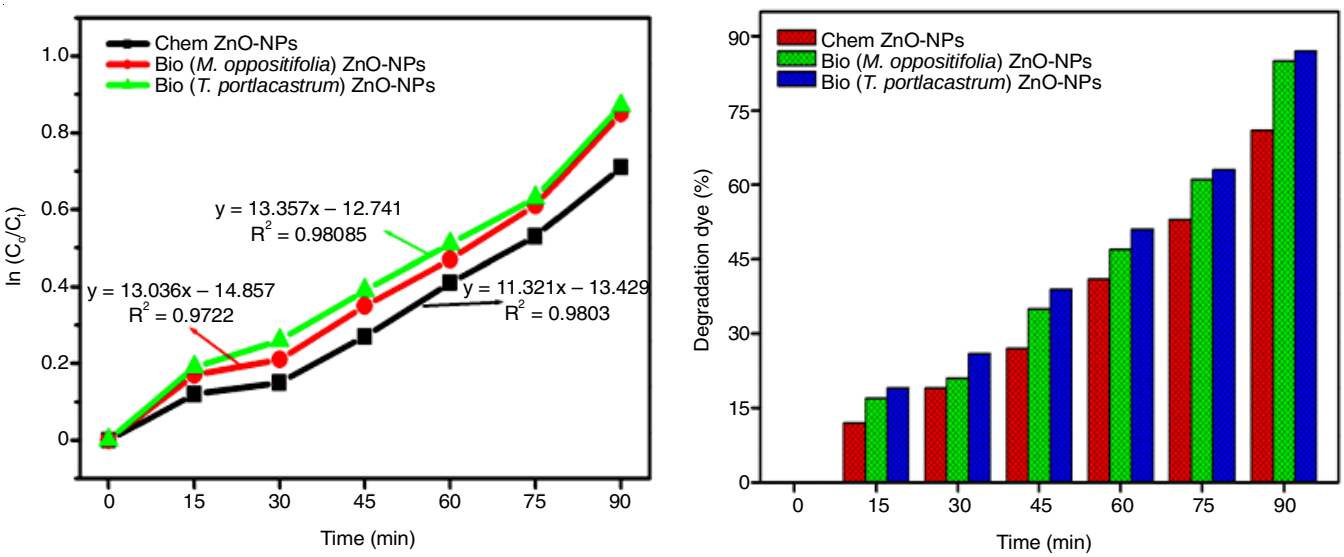

Fig. 9. Photodegradation of chemically synthesized La_2O_3 NPs and biosynthesized (*M. oppositifolia* and *T. portlacastrum* leaf extract) La_2O_3 NPs

TABLE-3
EFFECT OF ACID BLACK 1 DYE DEGRADATION BY CHEMICALLY AND BIOSYNTHESIZED (*M. oppositifolia* AND *T. portlacastrum* LEAF EXTRACT) La_2O_3 NPs

Time (min)	Degradation of dye (%)		
	La_2O_3 NPs		
	Chemically	*M. oppositifolia*	*T. portlacastrum*
0	0	0	0
15	12	17	19
30	19	21	26
45	27	35	39
60	41	47	51
75	53	61	63
90	71	85	87

having vacancies in oxygen present in the surface [23]. The photocatalytic mechanism of semiconductor materials continues the formation of electron-hole pairs (e^-, h^+) followed by electron and hole separation and reconnection. For chemically synthesized La_2O_3 NPs, the photocatalytic activity is attributed both to the donor states caused by many defect sites such as oxygen and interstitial zinc atoms and to the acceptor states resulting from zinc vacancies and interstitial oxygen atoms. For biosynthesized La_2O_3 NPs for acid black 1 dye colouring, however, electron-hole pairs are initially created and then species $^{\bullet}OH$ and $O_2^{\bullet}$ form [36]. Therefore, a better photocatalytic activity of semiconductor based nanoparticles must be avoided by recombining electron-hole pairs. The photocatalytic activities can be enhanced by controlled leaf extract over the La_2O_3 NPs up to a certain limit.

Kinetics studies: The kinetic study is conducted on the photodegradation of acid Black 1 dye by both chemically and biosynthesized La_2O_3 nanoparticles. The pseudo-first order rate proved that the rate constant for the acid black 1 dye degradation in the blended nanoparticles were always acceptable. The significant information in the plot of (C_o/C_t) as a function of irradiation time gives the rate constant values of 1.3429, 1.4897 and 1.2741 min^{-1} and the fitting correlation coefficient (R^2) is 0.9803, 0.9722 and 0.9801 for La_2O_3 NPs synthesized from *M. oppositifolia* and *T. portlacastrum* leaf extract (figure not shown). Finally, it is found that with increase of time there will be more increase of degradation. The experiment shown that the phytochemical constitutents present in leaf extract can significantly up the photocatalytic activities of La_2O_3 NPs.

Antibacterial activity: The antimicrobial activity of the synthesized nanoparticles were also evaluated against four bacteria *viz. Bacillus subtilis*, *Staphylococcus saprophyticus*, *Escherichia coli* and *Pseudomonas aeruginosa*. It was found that La_2O_3 NPs inhibited the growth of all of the tested bacteria. La_2O_3 NPs showed a higher toxicity for Gram-negative bacteria compared to Gram-positive bacteria. Moreover, biosynthesized nanoparticles were more effective than the chemically synthesized La_2O_3 NPs (Table-4).

TABLE-4
ANTIBACTERIAL ACTIVITY OF STUDIED PLANT LEAF EXTRACTS, CHEMICALLY SYNTHESIZED AND BIOSYNTHESIZED (*M. oppositifolia* AND *T. portlacastrum* LEAF EXTRACT) La_2O_3 NPs AT 50 µL

Bacteria	Zone of inhibition (mm)					
	M. oppositifolia	*T. portlacastrum*	Chemically La_2O_3 NPs	La_2O_3 NPs		Std
				M. oppositifolia	*T. portlacastrum*	
Bacillus subtilis	–	1	3	8	9	15
Staphylococcus saprophyticus	2	1	4	7	7	15
Pseudomonas aeruginosa	2	2	5	9	10	16
Escherichia coli	3	2	4	10	11	17

Conclusion

In summary, the chemically and plant mediated La_2O_3-nanoparticles have been successfully synthesized and characterized with XRD, FT-IR, HR-TEM, UV-DRS and PL measurements. In the light circular SAED pattern, which was consistent with the XRD results, a good polycrystalline cubic nature of the synthesized La_2O_3 NPs was obtained. Among the two studied plants mediated synthesized nanoparticles as photocatalyst, the *M. oppositifolia* mediated La_2O_3 NPs exhibited an excellent degradation performance of 87% for acid black 1 dye. Moreover, biosynthesized La_2O_3 NPs also showed the best activity in both Gram-negative and Gram-positive bacteria.

CONFLICT OF INTEREST

The authors declare that there is no conflict of interests regarding the publication of this article.

REFERENCES

1. Y. Verma, *Toxicol. Ind. Health*, **24**, 491 (2008); https://doi.org/10.1177/0748233708095769
2. R. Javaid and U.Y. Qazi, *Int. J. Environ. Res. Public Health*, **16**, 2066 (2019); https://doi.org/10.3390/ijerph16112066
3. J.O. Odiyo, L. Chimuka, M.A. Mamali and O.S. Fatoki, *Int. J. Environ. Sci. Technol.*, **9**, 203 (2012); https://doi.org/10.1007/s13762-012-0034-x
4. W.K. Dodds, *Limnol. Oceanogr.*, **51(1part2)**, 671 (2006); https://doi.org/10.4319/lo.2006.51.1_part_2.0671
5. E.A. Clarke and R. Anliker, Organic Dyes and Pigments, In: Anthropogenic Compounds. Springer: Berlin, Heidelberg, pp 181-215 (1980).
6. C. Comninellis, A. Kapalka, S. Malato, S.A. Parsons, I. Poulios and D. Mantzavinos, *J. Chem. Technol. Biotechnol.*, **83**, 769 (2008); https://doi.org/10.1002/jctb.1873
7. C. Zaharia, D. Suteu, A. Muresan, R. Muresan and A. Popescu, *Environ. Eng. Manag. J.*, **8**, 1359 (2009); https://doi.org/10.30638/eemj.2009.199
8. V. Homem and L. Santos, *J. Environ. Manage.*, **92**, 2304 (2011); https://doi.org/10.1016/j.jenvman.2011.05.023
9. C.Y. Teh, P.M. Budiman, K.P.Y. Shak and T.Y. Wu, *Ind. Eng. Chem. Res.*, **55**, 4363 (2016); https://doi.org/10.1021/acs.iecr.5b04703
10. S.G. Kumar and L.G. Devi, *J. Phys. Chem. A*, **115**, 13211 (2011); https://doi.org/10.1021/jp204364a
11. J. Herney-Ramirez, M.A. Vicente and L.M. Madeira, *Appl. Catal. B*, **98**, 10 (2010); https://doi.org/10.1016/j.apcatb.2010.05.004
12. B. Yan, *Acc. Chem. Res*., **50**, 2789 (2017); https://doi.org/10.1021/acs.accounts.7b00387
13. Y. Zhang, S. Liu, Z.-S. Zhao, Z. Wang, R. Zhang, L. Liu and Z.-B. Han, *Inorg. Chem. Front.*, **8**, 590 (2021); https://doi.org/10.1039/D0QI01191F
14. Z. Liu, Y. Li, Q. Bu, C.J. Guzy, Q. Li, W. Chen and C. Wang, *J. Power Sources*, **328**, 329 (2016); https://doi.org/10.1016/j.jpowsour.2016.07.096
15. E.E. Kiss and G.C. Boškovic, *Process. Appl. Ceram.*, **6**, 173 (2012); https://doi.org/10.2298/PAC1204173K
16. H. Tong, S. Ouyang, Y. Bi, N. Umezawa, M. Oshikiri and J. Ye, *Adv. Mater.*, **24**, 229 (2012); https://doi.org/10.1002/adma.201102752
17. A.J. Hoffman, E.R. Carraway and M.R. Hoffmann, *Environ. Sci. Technol.*, **28**, 776 (1994); https://doi.org/10.1021/es00054a006
18. A. Machulek Jr., S.C. Oliveira, M.E. Osugi, V.S. Ferreira, F.H. Quina, R.F. Dantas, S.L. Oliveira, G.A. Casagrande, F.J. Anaissi, V.O. Silva, R.P. Cavalcante, F. Gozzi, D.D. Ramos, A.P.P. da Rosa, A.P.F. Santos, D.C. de Castro and J.A. Nogueira, Application of Different Advanced Oxidation Processes for the Degradation of Organic Pollutants; In: Organic Pollutants Monitoring, Risk and Treatment, TECH Publisher: USA, Chap. 6, pp. 141-166 (2013).
19. K. Chand, D. Cao, D.E. Fouad, A.H. Shah, A.Q. Dayo, K. Zhu, M.N. Lakhan, G. Mehdie and S. Dong, *Arab. J. Chem.*, **13**, 8248 (2020); https://doi.org/10.1016/j.arabjc.2020.01.009
20. Mehilal, K.I. Dhabbe, A. Kumari, V. Manoj, P.P. Singh and B. Bhattacharya, *J. Hazard. Mater.*, **205-206**, 89 (2012); https://doi.org/10.1016/j.jhazmat.2011.12.022
21. M. Ghiasi and A. Malekzadeh, *Superlatt. Microstruct.*, **77**, 295 (2015); https://doi.org/10.1016/j.spmi.2014.09.027
22. A. Muthuvel, M. Jothibas and C. Manoharan, *J. Environ. Chem. Eng.*, **8**, 103705 (2020); https://doi.org/10.1016/j.jece.2020.103705
23. H. Kabir, S.H. Nandyala, M.M. Rahman, M.A. Kabir and A. Stamboulis, *Appl. Phys. A*, **124**, 820 (2018); https://doi.org/10.1007/s00339-018-2246-5
24. A. Muthuvel, M. Jothibas, C. Manoharan and S.J. Jayakumar, *Res. Chem. Intermed.*, **46**, 2705 (2020); https://doi.org/10.1007/s11164-020-04115-w
25. K.S. Babu, A.R. Reddy, C. Sujatha, K.V. Reddy and A.N. Mallika, *J. Adv. Ceram.*, **2**, 260 (2013); https://doi.org/10.1007/s40145-013-0069-6
26. N. Tripathi and S. Rath, *Mater. Charact.*, **86**, 263 (2013); https://doi.org/10.1016/j.matchar.2013.10.008
27. T. Marimuthu, N. Anandhan, M. Mummoorthi, and V. Dharuman, *AIP Conf. Proc*., **1731**, 080050 (2016); https://doi.org/10.1063/1.4947928
28. N. Sulaiman, Y. Yulizar, and D.O.B. Apriandanu, *AIP Conf. Proc*., **2023**, 020105 (2018); https://doi.org/10.1063/1.5064102
29. H. Saravani and M. Khajehali, *Orient. J. Chem.*, **31**, 2351 (2015); https://doi.org/10.13005/ojc/310464
30. M. Salavati-Niasari, G. Hosseinzadeh and F. Davar, *J. Alloys Comp.*, **509**, 134 (2011); https://doi.org/10.1016/j.jallcom.2010.09.006
31. E. Masarovicova and K. Kralova, *Ecol. Chem. Eng.*, **20**, 9 (2013); https://doi.org/10.2478/eces-2013-0001
32. G. Ravi, M. Sarasija, D. Ayodhya, L.S. Kumari and D. Ashok, *Nano Convergence*, **6**, 12 (2019); https://doi.org/10.1186/s40580-019-0181-6
33. S. Fiedler, L.O. Lee Cheong Lem, C. Ton-That and M.R. Phillips, *Appl. Surf. Sci.*, **504**, 144409 (2020); https://doi.org/10.1016/j.apsusc.2019.144409
34. Y. Kim and S. Kang, *Nanotechnology*, **22**, 275707 (2011); https://doi.org/10.1088/0957-4484/22/27/275707
35. H.W. Kim, J.C. Yang, H.G. Na and C. Lee, *Appl. Surf. Sci.*, **257**, 9420 (2011); https://doi.org/10.1016/j.apsusc.2011.06.022
36. W.R. Siah, H.O. Lintang and L. Yuliati, *Catal. Sci. Technol.*, **7**, 159 (2017); https://doi.org/10.1039/C6CY01991A